CCD Charge Density Study on Crystals with Large Unit Cell Parameters: The Case of Hexagonal L-Cystine

S. Dahaoui,[†] V. Pichon-Pesme,[‡] J. A. K. Howard,[†] and C. Lecomte*[,‡]

Crystallography Group, Department of Chemistry, University of Durham, South Road, Durham DH1 3LE, England, and Laboratoire de Cristallographie et Modélisation des Matériaux Minéraux et Biologiques (LCM³B), UPRESA CNRS 7036, Université Henri Poincaré, Nancy 1, Faculté des Sciences, B.P. 239, 54506 Vandoeuvre lès Nancy Cedex, France

Received: February 23, 1999

The electron density of L-cystine has been analyzed using 110 K single-crystal Mo Kα X-ray diffraction data to a resolution of $(\sin\theta/\lambda)_{max} = 1.123$ Å^{-1} with a CCD area detector. Due to the large *c*-parameter (55.9 Å), a discussion is made for choosing the best experimental data collection strategy and data reduction. A multipolar pseudo-atom density model was fitted against the 2309 observed data with $I > 3\sigma(I)$, [$R(F) = 0.014$, $R_w(F) = 0.019$, $S = 0.73$]. The deformation density distribution and topological analysis of charge density clearly reveals disulfide bridge characteristic features and sulfur lone pair electron regions which validate high-level ab initio calculations. The valence shell charge concentration (VSCC) suggests sp^3 hybridization of sulfur atoms.

I. Introduction

The structures and properties of molecules containing sulfur−sulfur bonds have been of interest for decades. It is known that the disulfide linkage plays an important role in protein, enzyme, and antibiotic structure stabilization and in the biological activity of molecules. These properties are related to the ability of the sulfur−sulfur interaction to be formed or broken. The mechanism involved in these processes, which is not well understood, is important in chemistry and biochemistry. Then in this work we study the experimental charge density distribution of the disulfide amino acid L-cystine. This latter molecule has also been shown to protect the body against damage induced by alcohol and cigarette smoking as a detoxification agent.[1]

The experimental electron distribution in S−S interactions were first studied in the 1970s. In 1977, Coppens et al.[2] reported the first experimental charge density distribution in octasulfur S_8 by X-ray and neutron diffraction. In that work the deformation density was found to have[2] "a contraction at about 0.6 Å from the nucleus and an expansion near the nucleus" [S−S = 2.05 Å]. A comparison was made with an ab initio calculation on H_2S_2 [S−S = 2.055 Å], but no contraction of the density appeared in the theoretical maps. Other experimental studies by Kirfel et al.[3] on $Na_2S_2O_6{\cdot}2H_2O$ and $Na_2S_2O_6{\cdot}2D_2O$ indicated a maximum in the deformation density distribution in the middle of the S−S bonds [S−S = 2.14 Å]. In 1983, Elerman and al.[4] investigated the S−S bonds in magnesium thiosulfate hexahydrate ($MgS_2O_3{\cdot}6H_2O$) and peaks of about 0.25 e A^{-3} were also observed at the midpoint between the sulfur atoms [S−S = 2.02 Å]. Molecular structures and molecular geometries were determined in SCF calculations, with STO-3G and 6-21G* basis sets, for several systems by Tang and co-workers[5] in 1985. The chemical bonds were then defined and classified in terms of properties of the total charge distribution. Wang and co-workers[6−12] investigated the S−S bonds in several thiathiophthene derivatives [S−S = 2.04−2.51 Å] and concluded that there was little density accumulation in the S−S bonds; their theoretical calculations, based on the extended Hückel molecular orbital (EHMO) model, were, as we could expect, unable to describe appropriately the electron density distribution in these systems. Recently, extended ab initio SCF studies were performed by Brown and Smith[13] to examine the charge density of the S−S bonds in nine different systems, H_2S_2, S_2, S_3, S_4, S_6, S_8, 2,5-dimethyl-6a-thiathiophthene (DMT), tetramethylthiuram disulfide (TMTD), and S_4N_4 [S−S = 2.055, 1.889, 1.930, 2.089, 2.068, 2.048, 2.351, 2.008 and 2.593 Å, respectively]. These calculations highlight the necessity for the inclusion of d polarization functions for the sulfur atoms in the computational basis set. These latter authors showed also that electron correlation effects flatten out the deformation density by a maximum of 0.04 e Å^{-3} in the midpoint of the S−S bonds. Comparisons between these theoretical calculations and experimental electron distribution maps were made for S_8, DMT, TMTD, and S_4N_4. Some double peaks existing in the S−S experimental maps were not reproduced by the theoretical calculations. Finally in 1996, McCormack et al.[14] reported experimental and theoretical studies of the charge density distribution in 3,3,6,6-tetramethyl-*S*-tetrathiane. From the topological analysis of the charge density, these authors described the S−S bonds [S−S = 2.023 Å] as weak covalent interactions. The need for inclusion of sulfur atom d orbitals in order to explain the nature of S···O interaction in short X−S···O contact has also been published by Cohen-Addad et al.[17] In that study the S···O interaction was explained in detail by the *σ*-type bond interaction between the oxygen p and the sulfur p and d orbitals. The observed variation of the S···O distance with the nature of the atom bonded to S was explained in terms of the strength of the coupling between the X−S antibonding orbital and the oxygen lone-pair orbitals.

To gain more insight in the S−S interaction, we describe here the experimental charge density study of L-cystine and we

* Author to whom correspondence should be addressed. E-mail: lecomte@lcm3b.u-nancy.fr.
[†] University of Durham.
[‡] Université Henri Poincaré.

10.1021/jp990641k CCC: $18.00
Published on Web 07/16/1999

TABLE 1: Experimental Details

Crystal Data	
chemical formula	$C_3H_6NO_2S$
temperature (K), radiation type, wavelength (Å)	110, Mo Kα, 0.71073
cell setting, space group	hexagonal, $P6_122$
$a = b$ (Å), c (Å), V (Å^3), Z, D_x (g·cm^{-3})	5.412 (1), 55.956 (1), 1419 (2), 12, 1.685
crystal form, size (nm^3), color	hexagonal prism, 0.22 × 0.18 × 0.06, colorless
μ (mm^{-1})	0.553
Data Collection	
diffractometer	Siemens-Bruker CCD
data collection method, data reduction	ω-scan, SAINT software
absorption correction, T_{min}, T_{max}	Gaussian quadrature (ABSORB[31]), 0.895, 0.967
number of frames	22 844
number of measured reflections, completeness	72 851, 100%
hkl limit, $[(\sin\theta/\lambda)]_{max}$ (Å^{-1})	$-12 \rightarrow h \rightarrow 12$, $-12 \rightarrow k \rightarrow 11$, $-125 \rightarrow l \rightarrow 125$, 1.123
R_1, R_2, R_w, S (see Table 2 for definition)	0.059, 0.036, 0.125, 1.246

characterize the disulfide linkage by topological analysis of the electron density distribution. This study was a considerable challenge to obtain accurate single crystal diffraction data, using a CCD area detector, for a compound with such large cell parameters as L-cystine ($c = 55.956(1)$ Å). The charge density data on sulfur atoms will also be deposited in our data bank of experimental density parameters.[18,19]

II. Data Collection and Data Reduction Analysis

It is well-known that charge density studies need accurate X-ray diffraction measurements and careful data reduction. This step, which requires considerable experimental expertise, is very time consuming when using a conventional four-circle diffractometer equipped with a scintillation-point detector. Two-dimensional (2D) detectors like CCD or imaging plates (which are widely used in protein crystallography) are also becoming more and more popular for small molecule structure determinations (2−24 h data collection). However, until recently very few electron density studies have been obtained from 2D-detector data.[20−27]

II.1. Preliminary Short Data Collection. Crystals of hexagonal and tetragonal forms of L-cystine were grown by slow evaporation of an aqueous solution of ammonium hydroxide in a molar ratio of 1:6. A good-quality hexagonal-shaped crystal (0.22 × 0.18 × 0.06 mm^3) was selected for the X-ray diffraction study. The sample displayed eight faces: {1 0 0}, {−1 0 0}, {1 −1 0}, {−1 1 0}, {0 1 0}, {0 −1 0}, {0 0 1}, and {0 0 −1}. Because of the large c-parameter ($c = 55.956$ (1) Å), a preliminary short and quick data collection on a Siemens SMART CCD-based diffractometer at room temperature with Mo Kα radiation was undertaken. The aim of this procedure was to define the best strategy for X-ray data collection. Key questions when using the SMART CCD-based diffractometer are as follows:

Along which direction the crystal would be glued? This question arises because the Siemens CCD diffractometer possesses only three Eulerian circles (ω, φ, θ) with χ fixed at 54.74°.

Which crystal-to-detector distance D will be chosen?

Which 2θ positions give high-resolution data?

Which scan width and what exposure time give the most accurate intensity?

How can 100% data completeness be obtained and with what redundancy?

To answer these questions, different preliminary tests were essential. Due to the large c-parameter, the first test was made with crystal-to-detector distance $D = 11$ cm and with the crystal attached to glass fiber with grease with the c-axis perpendicular to the goniometer φ-axis. In this case the orientation matrix could be obtained without any problems. The ASTRO program[28] used to check the planned data collection gave completeness of 95% in a given resolution of 55° in 2θ [$(\sin\theta/\lambda)_{max} = 0.65$ Å^{-1}]. In the second test, the same crystal was glued with the c-axis parallel to the φ-axis of the goniometer head. In that case it was impossible to obtain the orientation matrix and consequently the cell parameters. In the third test, the crystal was glued obliquely, i.e., ∼ 20° between the (0 0 1) face and the φ-axis. The data were then collected and were 100% complete to the same resolution as above. With this last orientation, the crystal-to-detector distance was gradually increased from 6 to 17 cm in order to determine the best compromise between nonoverlapping reflections and good accuracy for weak intensities. We found $D = 8$ cm to be a good distance.

II.2. Data Collection Strategy. The crystal was cooled to 110 K with an Oxford Cryostream N_2 open flow cryostat. Three batches of data were collected using Mo Kα radiation at three detector positions: the first two at 20 and 54° in 2θ (low angle) and the third at 88° in 2θ (high order). Twenty seconds (20s) frames were measured for the first batch, 30s for the second, and 50s for the third one because of the decrease in the diffracted intensity at high 2θ values. The maximum redundancy in the data was obtained using a combination, for each batch, of eight sets of runs: each set had different φ angles (0, 45, 90, 135, 180, 225, 270, and 315°) and each frame covered 0.2° in ω in order to have accurate intensity profiles. The crystal decay was monitored by repeating the 50 initial frames at the beginning and at the end of the data collection for each batch and analyzing the duplicate reflections. The complete data collection strategy is summarized in Table 1. A total of 22 844 frames was collected over a period of 17 days. During the data collection, no low-temperature problem occurred.

II.3. Data Reduction. The unit cell parameters were refined using SMART software[28] on 512 reflections of the two low angle batch only [$0.5 < \sin\theta/\lambda < 0.8$ Å^{-1}], with a threshold $I/\sigma(I) > 30$. Data reduction was performed using SAINT which corrects for Lorentz, polarization effects.[28] The procedure of integration of frames was described by Kabsch.[29] Each three-dimensional peak profile was placed inside a three-dimensional box of a given size. The size of the box is constant for all low-angle frames and $1^1/_2$ larger in terms of peak width (x and y directions) for high order frames because of the $K\alpha_1$ and $K\alpha_2$ splitting. The intensities have been corrected for decay using SADABS.[30] The absorption is not negligible with Mo Kα radiation ($\mu = 0.553$ mm^{-1}), and the intensities have been corrected using ABSORB program.[31] The minimum and the maximum transmission factors are $T_{min} = 0.895$ and $T_{max} = 0.967$.

TABLE 2: Statistics on Multiple Reflections[a]

	n	m	$\langle n\rangle$	R_1	R_2	R_w	S
all data	72085	5464	13.2	0.059	0.036	0.125	1.246
$Q > 0$	70962	5308	13.4	0.058	0.036	0.121	1.236
$Q > 1$	62772	4371	14.4	0.053	0.035	0.106	1.194
$Q > 2$	54490	3443	15.8	0.048	0.034	0.093	1.159
$Q > 3$	48763	2865	17.0	0.045	0.034	0.084	1.137
$Q > 4$	43791	2401	18.2	0.043	0.034	0.076	1.109
$Q > 6$	36025	1765	20.4	0.039	0.033	0.065	1.075
$s < 0.083$	8	1	8.0	0.019	0.028	0.021	0.838
$s < 0.333$	5085	153	33.2	0.027	0.031	0.072	1.244
$s < 0.500$	15091	508	29.7	0.031	0.032	0.085	1.270
$s < 0.667$	30609	1174	26.1	0.037	0.033	0.097	1.259
$s < 1.000$	63052	3969	15.9	0.054	0.035	0.117	1.238
$s < 1.250$	72085	5464	13.2	0.059	0.036	0.125	1.246

[a] n and m are the number of reflections and the number of the unique reflections, respectively. w is the robust/resistant Tukey weight (see ref 32). $\langle n\rangle$ is the average measurement multiplicity. $s = \sin\theta/\lambda$ (Å^{-1}) and $Q = I/\mathrm{Max}(\sigma_{int},\sigma_{ext})$.

$$R_1 = \sum_H \left[\frac{n}{n-1}\right]^{1/2} \sum_I |I - \bar{I}| / \sum_H \sum_I |I|,$$

$$R_2 = \left\{\sum_H \left[\frac{n}{n-1}\right] \sum_I (I - \bar{I})^2 / \sum_H \sum_I I^2\right\}^{1/2}$$

$$R_w = \left\{\sum_H \left[\frac{n}{n-1}\right] \sum_I w[(I - \bar{I})/\sigma(I)]^2 / \sum_H \sum_I w[I/\sigma(I)]^2\right\}^{1/2},$$

$$S = \left\{\left(\frac{n}{n-m}\right) \sum_H \left[\frac{n}{n-1}\right] \sum_I w[(I - \bar{I})/\sigma(I)]^2 / \sum_H \sum_I w\right\}^{1/2}$$

$$\bar{I} = \sum (wI) / \sum w, \quad \sigma_{int} = \left\{\left[\frac{n}{n-1}\right] \left(\sum_H w(I - \bar{I})^2 / \sum_H w\right)\right\}^{1/2},$$

$$\sigma_{ext} = \{\sum_H w\sigma(I)^2 / \sum_H w\}^{1/2}$$

II.4. Averaging Data. Of the 72 851 integrated reflections, only 699 reflections were rejected as abnormal outliers. Sixty-seven reflections were measured only once, 112 were measured twice, and 5352 are multiple measurements which, on averaging in point group 622 using the new version of SORTAV program[32] adapted for area detector data, gave 5531 unique structure factor amplitudes to a resolution of $(\sin\theta/\lambda)_{max} = 1.123$ Å^{-1} corresponding to an average redundancy of 13 (26 for $\sin\theta/\lambda < 0.7$ Å^{-1}). Internal agreement factors for all data (definitions are given in Table 2) are $R_1(F^2) = 0.059$, $R_2(F^2) = 0.036$, $R_w(F^2) = 0.125$, and $S = 1.246$ compared to $R_1(F^2) = 0.066$, $R_2(F^2) = 0.033$, $R_w(F^2) = 0.128$, and $S = 1.281$ before absorption correction confirming the usefulness of this correction. Careful examination of the 72 152 measured reflections showed that 1123 intensities are negative and that 27 171 reflections have $I < 4\sigma(I)$, which explains the high values of the agreement factors R_1, R_2, R_w, and S for all data. Nevertheless, as shown in Table 2, the low order internal agreement is very good for $\sin\theta/\lambda < 0.7$ Å^{-1}. To assess the statistical distribution of our multiple data, a normal probability plot as described by Abrahams et al.[33] was made for reflections which were measured more than 40 times. Figure 1. gives an example for the (1 0 9) reflection. It shows that the observed deviation $(F_{obs} - F_{mean})/\sigma$ is close to the expected normal distribution. A bivariate analysis based on the ratio $\sigma_{int}/\sigma_{ext}$ as a function of the magnitude of intensities and of resolution was carried out to obtain adjusted error estimates $\sigma(I)$. The minimum and the maximum values of $\sigma_{int}/\sigma_{ext}$ obtained were 1.05 and 1.14, respectively. Because of the great number of negative and weak reflections, the BAYES program[32] was used. As mentioned by Rees[34] and by French and Wilson,[35] the small and negative intensities are due to the overestimation of the background and these intensities (especially for $I < 5\sigma(I)$) can be corrected using *Bayes theory*. However, to avoid modeling the noise, we decided to use in the least-squares refinement the 2309 reflections having $I \geq 3\sigma(I)$ which were considered to be accurately observed.

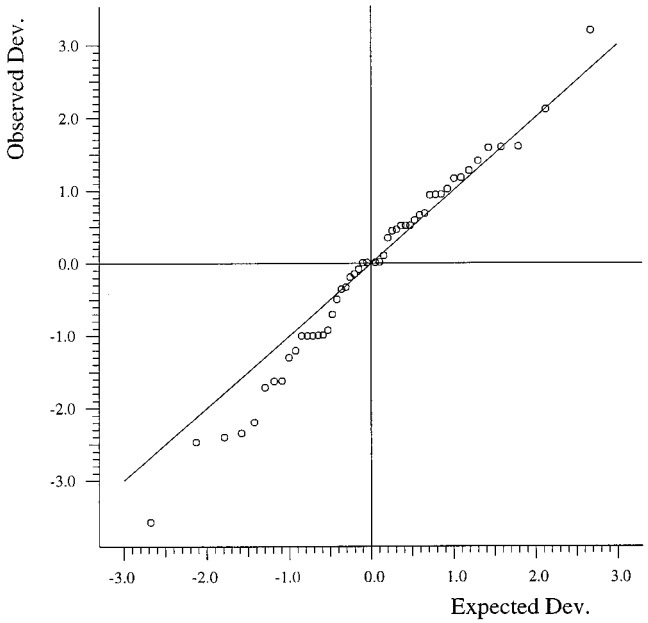

Figure 1. Normal probability plot of $[(F_{obs} - F_{mean})/\sigma]$ for the (109) reflection measured 50 times.

III. Least-Squares Refinements

III. 1. Conventional Refinement. The crystal structure at room temperature of hexagonal L-cystine was first reported by Oughton and Harrison[36] and solved to $R = 0.123$ by three-dimensional methods. However, we solved the structure at 110 K by direct methods using the SHELXS86 program;[37] the spherical atom refinement was performed with SHELXL93[38] on F^2. All H atoms were located by difference Fourier synthesis. The refined parameters ($N_{par} = 88$) included anisotropic mean square displacements for non-H atoms, and positions and isotropic mean square displacements for H atoms ($R(F^2) = 0.0335$ with all data). The Flack parameter[39] equal to 0.07 (5) confirms the L-configuration of the structure.

III.2. High-Order and Hydrogen Atom Refinements. A high order refinement (HO) was performed, using 789 reflections with $0.8 < \sin\theta/\lambda < 1.123$ Å^{-1} and $I > 3\sigma(I)$, to obtain the best estimate of the atomic positions and thermal displacement parameters of the non-H atoms. For non-H atoms, *xyz* and U^{ij} were refined ($N_{par} = 64$). Convergence was achieved at $R(F) = 0.026$, $R_w(F) = 0.032$, and $S = 0.91$. At the end of the HO refinement, the rigid-bond test[40] was applied for non-H atoms: the test gave promising results with a maximum discrepancy $\Delta Z^2 = 15 \times 10^{-4}$ Å^2 for the C3−O1 bond. Because of the relatively high thermal anisotropy of S, O1, and O2 atoms, an anharmonic model was tested but no improvement was observed in the agreement indices, the anharmonic parameters C^{ijk} and D^{ijkl} being less than their standard deviations. At the end of the HO refinement the residual experimental deformation density calculated in the C1−S−S^A (S^A: x, $2 + x - y$, $^1/_6 - z$) and C3−O1−O2 planes does not show any contour greater than the estimated error 0.05 e Å^{-3}.

The positional and isotropic thermal parameters of H atoms were refined together with the scale factor and the isotropic extinction parameter[41] at low angle ($\sin\theta/\lambda < 0.8$ Å^{-1}, 1520

TABLE 3: Agreement Indices with (a) MOLLY[43] and (b) XDLSM[50] [a]

(a) Agreement Indices with MOLLY

n_l ($l = 1, 4$)	α	$\kappa'\alpha$	$R(F)$	$R_w(F)$	S	$\sum_w\Delta^2$	k^{-1}
4 4 6 8	3.85	4.09(12)	0.0142	0.0202	0.724	1103	0.1110(1)
	4.10	4.48(12)	0.0141	0.0193	0.723	1099	0.1110(1)
	4.40	4.58(13)	0.0142	0.0201	0.723	1101	0.1110(1)

(b) Agreement Indices with XDLSM

n_l ($l = 1, 4$)	α	$\kappa_1'\alpha$	$\kappa_2'\alpha$	$\kappa_3'\alpha$	$\kappa_4'\alpha$	$R(F)$	$R_w(F)$	S	$\sum_w\Delta^2$	k^{-1}
4 4 6 8	3.85	3.85(10)	3.33(5)	3.17(5)	3.84(6)	0.0143	0.0203	0.728	1114	0.1110(1)
	4.10	4.29(11)	3.55(5)	3.41(6)	4.33(6)	0.0142	0.0194	0.725	1107	0.1110(1)
	4.40	4.36(11)	3.59(5)	3.45(6)	4.43(6)	0.0142	0.0202	0.725	1107	0.1110(1)

[a] $R(F) = \sum\Delta/\sum F_{obs}$, $R_w(F) = [(\sum w\Delta^2)^2/\sum wF_{obs}^2]^{1/2}$, $S = [(\sum w\Delta^2)^2/N_{obs} - N_{par}]^{1/2}$, $\Delta = k^{-1}F_{obs} - F_{calc}$, $w = 1/\sigma^2(F_{obs})$; α in bohr^{-1}; number of data $N_{obs} = 2309$, number of refined parameters $N_{par} = 205$ ($N_{obs}/N_{par} = 11.3$).

reflections with $I > 3\sigma(I)$) giving $R(F) = 0.021$, $R_w(F) = 0.027$, and $S = 1.08$ for 26 refined parameters; then the hydrogen atoms were shifted by extending along the C(sp^3)−H and N−H bond vectors to average bond distance values determined from neutron-diffraction studies,[42] respectively to 1.085 and 1.032 Å.

III.3. Multipolar Refinements. Multipolar refinements were performed using the Hansen−Coppens model.[43] The electron density of an atom is described by

$$\rho_{atom}(\mathbf{r}) = \rho_{core}(r) + P_v\kappa^3\rho_v(\kappa r) + \sum_{l=0}^{l_{max}}\kappa'^3 R_{n_l}(\kappa' r)\sum_{m=0}^{l} P_{lm\pm} y_{lm\pm}(\theta,\varphi)$$

where ρ_{core} and ρ_v are the spherically averaged core and valence electron density. y_{lm} represents the multipolar spherical harmonic angular functions in real form, R_{n_l} the Slater type radial functions, and κ and κ' are the contraction/expansion coefficients of the perturbed density. The local atom-centered Cartesian axes are given as Supporting Information. P_v is the refined valence population parameter, which gives the charge transfer with respect to the number N_v electrons in the valence orbitals of the free atom. The multipole expansion was truncated at the hexadecapole level for S (to take care of possible d orbital polarization), at the octopole level for O and C atoms, and to one single dipole along the C(N)−H bond centered on the hydrogen atom. The multipolar refinement was carried out on F using all 2309 reflections with $I > 3\sigma(I)$ and $\sin\theta/\lambda < 1.123$ Å^{-1} with the following strategy: scale factor; P_v then κ, P_v, and κ; P_{lm} then κ'; xyz and U^{ij} for the non-H atoms. The unit cell was constrained to be neutral. Initially, to decrease the number of variables and to reduce any possible phase problem,[44] noncrystallographic molecular symmetry was used to constrain chemically equivalent atoms to have identical deformation density. Then, when convergence was reached, the constraints were released, and all positional and thermal parameters were refined together with the multipolar parameters (except κ and κ' of H atoms) until convergence. At each step, the H-atom coordinates were shifted to neutron diffraction values[42] and hydrogen isotropic thermal displacements were adjusted at low order ($\sin\theta/\lambda < 0.8$ Å^{-1}).

III.4. Test of the Sulfur Radial Function Parameters. The exponential-type radial functions $R_{n_l}(\kappa' r)$, controlled by the refined expansion/contraction κ' parameter, are defined by

$$R_{n_l}(r) = \frac{(\kappa'\alpha)^{n_l+3}}{(n_l+2)!} r^{n_l} e^{-\kappa'\alpha r}$$

For each atom, $n_l \geq l$ and $\alpha = 2\langle\xi\rangle$, where $\langle\xi\rangle$ is the averaged orbital exponent from the ground states of the valence orbitals wave functions calculated for a HF-SCF free atoms.[45] For the first-row atoms, combination of Poisson's law[46] and atomic orbital product arguments suggests the n_l values of 2, 2, 3 for $l = 1$, 2, and 3. In our refinements, the n_l parameters used were 2, 2, 3 for C, O, N, and H atoms and α values were 3.0, 4.5, 3.8, and 2.26 bohr^{-1}, respectively. For the second-row atoms, recent analysis has shown that the Slater radial function must be optimized:[47−49] in BTDMTTF-TCNQ, Espinosa et al.[48] have proposed a common value ($\alpha = 4.1$ bohr^{-1}) independent of the l ($l = 1-4$) parameter due to the limitations of the MOLLY program. To check the dependence of α as a function of l, XDLSM of the XD package[50] was used to refine the data: in this program, each atomic multipolar function may have distinct α parameters by refining κ'_l parameters ($l = 1$ for the dipole to 4 for the hexadecapole in the case of sulfur). Least-squares refinement statistics of fit and the values of the refined $\alpha'_l = \kappa'_l\alpha$ obtained at the end of the multipolar refinements are given in Table 3 and in Supporting Information. These tables show that there is no need to use α dependent on l. As found also by Espinosa et al.,[48] the R factors are equal for all models. For each set, no statistically significant changes are found in the minimized function $\sum_w\Delta^2$ nor for the scale factors at convergence. Only the inspection of the experimental residual maps around the sulfur atom shows certain differences. Indeed, all residual maps in the C1−S−S^A plane systematically exhibit positive residual density at a distance of 0.65 Å, perpendicular to the S−S^A disulfur bridge and a density peak at 0.5 Å from S^A in the lone-pair region. The difference between all residual maps are small, less than 0.1 e Å^{-3} as expected from the $\sum_w\Delta^2$ values. The lowest residual was obtained with the following $n_l = 4, 4, 6, 8$, $\alpha = 4.1$ bohr^{-1} parameters. Those sulfur parameters were kept for the final refinements for which agreement factors are given in Table 3. The fractional coordinates, thermal parameters, P_v, κ, P_{lm}, and κ' parameters of the final converged model have been deposited as Supporting Information. Convergence was achieved at $R(F) = 0.014$, $R_w(F) = 0.019$, and $S = 0.72$ (see Table 3a).

IV. Results and Discussion

IV.1. Crystal Structure. Figure 2. gives an ORTEP view[51] of the molecular packing. Selected bond lengths and angles after multipolar refinement are given in Table 4. A disulfide bridge occurs between two cystine molecules related by a 2-fold axis parallel to [1 0 0] or [1 1 0] (S−S^A = 2.0472 (4) Å). The cystine molecule has a right-handed disulfide chirality. The disulfide dihedral angle (C1−S−S^A−C1^A) is 75.18 (5)°. This angle is not significantly different from the average, 75.5 (2.5)°,

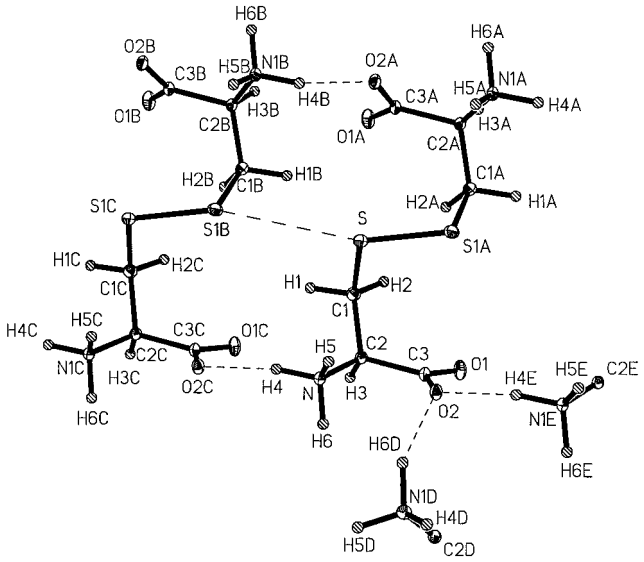

Figure 2. ORTEP view of $C_3H_6NO_2S$, with 50% probability thermal ellipsoids for non-H atoms. Symmetry codes for molecules: (A) x, $2 + x - y$, $^1/_6 - z$; (B) x, $1 + x - y$, $^1/_6 - z$; (C) x, $-1 + y$, z; (D) $1 + x - y$, $2 - y$, $-z$; (E) x, $1 + y$, z. Intermolecular bonds are indicated by dotted lines.

TABLE 4: Selected Bond Lengths (Å) and Angles (deg) for L-Cystine at 110 K (Multipolar Model)[a]

S−S^A	2.0472(4)	C1−S−S^A	104.15(2)
S−C1	1.8178(7)	O1−C3−O2	125.73(7)
C3−O2	1.267(1)	O1−C3−C2	17.25(7)
C3−O1	1.245(1)	O2−C3−C2	117.01(6)
C3−C2	1.5378(9)	N−C2−C1	112.05(5)
C2−N	1.480(1)	N−C2−C3	109.67(5)
C2−C1	1.523(1)	C1−C2−C3	113.39(5)
S···S^B	3.4264(4)	C1−S−S^A−C1^A	75.18(5)

D−H···A	H···A	D···A	D−H···A
N−H4···O2^C	1.777(1)	2.785(1)	164.40(5)
N−H6···O2^D	1.910(1)	2.827(1)	146.28(4)
N−H5···O1^G	1.844(1)	2.803(1)	153.22(5)

[a] Symmetry codes: (A) x, $2 + x - y$, $^1/_6 - z$; (B) x, $1 + x - y$, $^1/_6 - z$; (C) x, $y - 1$, z; (D) $1 + x - y$, $2 - y$, $-z$; (G) $1 + x$, y, z.

computed from the Cambridge Structural Database (CSD)[52] for all occurrences of the C(sp^3)−S−S−C(sp^3) fragment (166 structures observed, December 1998). Also, the average bond length taken over a large number of sulfur−sulfur bonds of the CSD is found to be 2.039 (2) Å, close to the 2.0472 (2) Å value for L-cystine (Figure 3a). The differences in S−S bond lengths in the C−S−S−C moiety are partly due to the lone-pair repulsion between the two S atoms which is most pronounced when the dihedral Φ angle is close to zero and partly due to the π bonding which is maximum for Φ around 90°. These features are well reproduced in Figure 3b, which shows that Φ increases when the S−S bond length decreases.

The S···S^B (S^B: x, $1 + x - y$, $^1/_6 - z$) intermolecular contact found in L-cystine (3.4264 (4) Å) is much shorter than the sum of van der Waals radii (3.7 Å): From the 166 entries of the CSD we found only 40 structures containing a C(sp^3)−S−S−C(sp^3) fragment which have intermolecular S···S^B contacts smaller than the sum of van der Waals radii. The search was carried out using $3.2 < S\cdots S^B < 3.7$ Å. As defined recently by Allen et al.,[53] the directionality parameters θ and φ describing the direction of approach of one S^B atom to the plane containing the other S lone pairs, are calculated for each structure. A sp^3 hybridization of the sulfur atom would suggest that θ and φ angles of 0° and 120° respectively indicate the direction of the lone pairs and of the S···S^B vector. A polar histogram of θ versus φ from the database analysis is given in Figure 3c. This figure reveals a systematic trend of crystallographic data: S···S^B contacts tend to be formed out of the plane containing the sulfur lone pairs. There is a clear preference for θ angle close to +37° and for φ angles close to ±160°. Our results ($\theta = 35°$ and $\varphi = -163°$) for the L-cystine at 110 K are in line with the distribution of the experimental values derived from CSD. The positive θ angles and the negative φ angles found systematically indicate that there is a higher probability for formation of short C−S−S···S^B contact collinear to the S−S bonds. This phenomenon[54] has been interpreted as a S interaction with the lowest unoccupied molecular orbital (LUMO) σ^*(S−S).

IV.2. Charge Density and Topology. The experimental residual density maps (Figure 4) do not show any contour greater than 0.1 e Å^{-3}, indicating that the noise level in the experimental data is low and confirming the high quality of the data. The Hirshfeld rigid-bond test[40] carried out after the multipolar refinement is also good, giving maxima mean-square-displacement amplitudes along the bond directions less than 10^{-3} Å^2 except for the C3−O1 bond ($\Delta Z^2 = 1.6 \times 10^{-3}$ Å^2). This analysis indicates that the multipole refinement yielded an effective deconvolution of the mean-square atomic displacements from the valence electron density deformation.

The experimental deformation density (see maps for definition) in the C1−S−S^A plane, in the plane bisecting the C1−S−S^A angle, and in the plane containing the S−S^A bond, and the c-axis, is given in parts a, b, and c, respectively, of Figure 5. These maps were calculated using 1893 observed reflections with $\sin\theta/\lambda < 0.9$ Å^{-1} and $I > 3\sigma(I)$. The bonding density in both C1−S and C1−H1 bonds is 0.30 (5) e Å^{-3}. One single peak of deformation density of about 0.15 e Å^{-3} is found at the midpoint of the S−S^A bond. The sulfur features appear at the same position but slightly weaker (<0.05 e Å^{-3}) on the static maps (see Supporting Information). This can be attributed to the difficulty of describing the sulfur radial function (∼ 0.10 e Å^{-3} in the S−S bond in residual map Figure 4). The general features of the S−S deformation density are in good agreement with those described by Coppens et al.[2] in their experimental study of S_8 and by Wang and co-workers in the X−X study of some thiathiophthene derivatives.[6−12] In this latter case, the static S−S bonding density modelized via the multipole model was also smaller than the dynamic one. Kirfel at al.[3] in their experimental work on the $[S_2O_6]^-$ anion reported a higher density single peak in their S−S dynamic map (∼0.40 e Å^{-3}) which split into two bumps separated by 0.87 Å on the static map. However, as specified by the authors, their experimental resolution ($d_{min} = 0.71$ Å, $(\sin\theta/\lambda)_{max} = 0.7$ Å^{-1}) does not allow a conclusion; furthermore this feature may also be due to an overparametrization of the Hirshfeld[55] model. In the L-cystine case, even if the static density is slightly weaker than the dynamic one, at least the nature (single or double peak) and the position of the bonding features are the same on both dynamic and static maps for a much higher resolution ($d_{min} =$ 0.44 Å). Therefore, those data agree only with a single peak description for the S−S deformation density; this single peak of ∼ 0.15 e Å^{-3} validates the ab initio calculations of Brown and Smith.[13] The sulfur atom lone pairs are very well resolved, as shown in Figure 5b, with two peaks of 0.25 (5) and 0.30 (5) e Å^{-3} at ∼ 0.6 Å from the nucleus. Finally the deformation density in the C−C, C−N, and C−O bonds agree quantitatively with our previous peptide X-ray diffraction and ab initio SCF studies.[56−59]

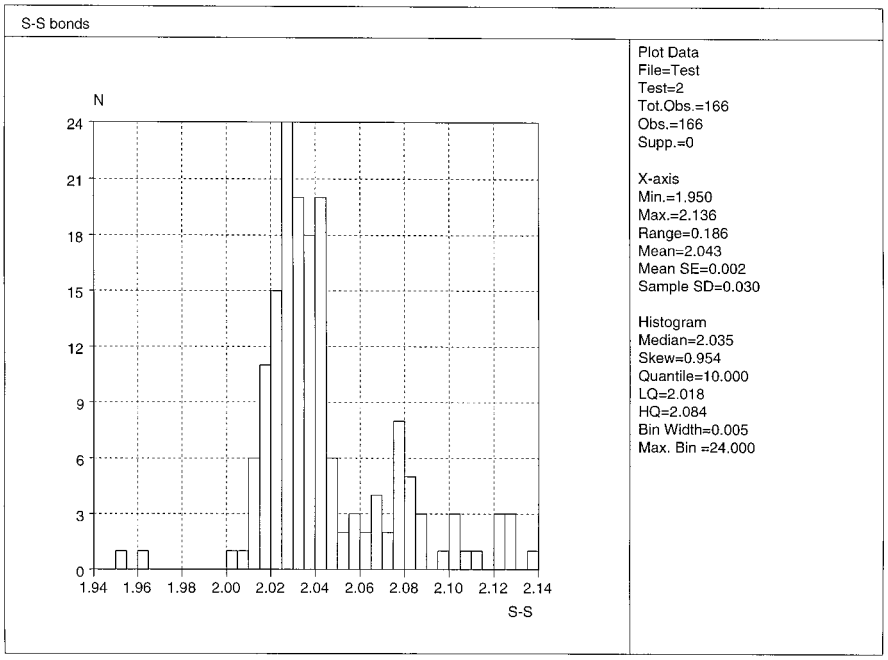

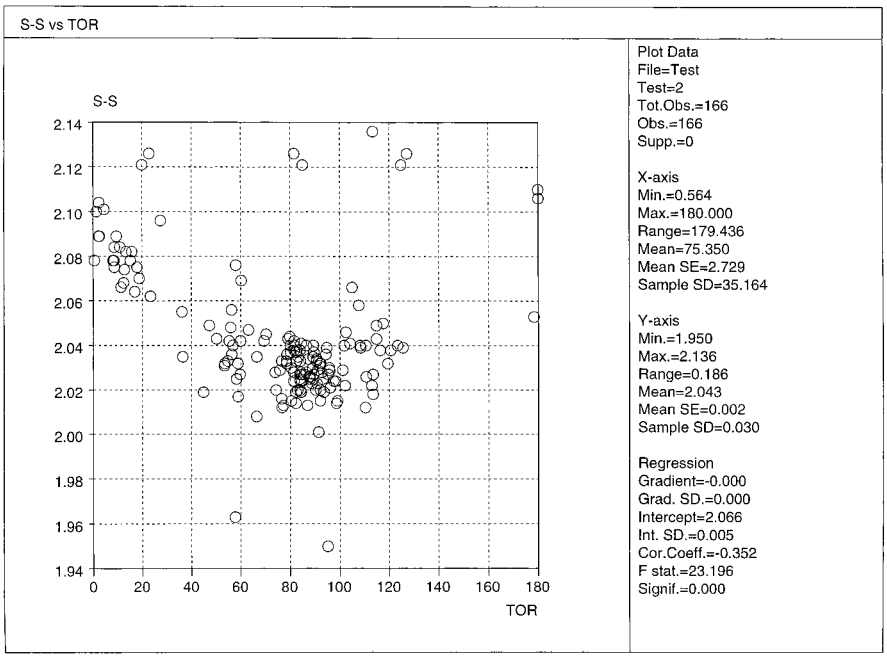

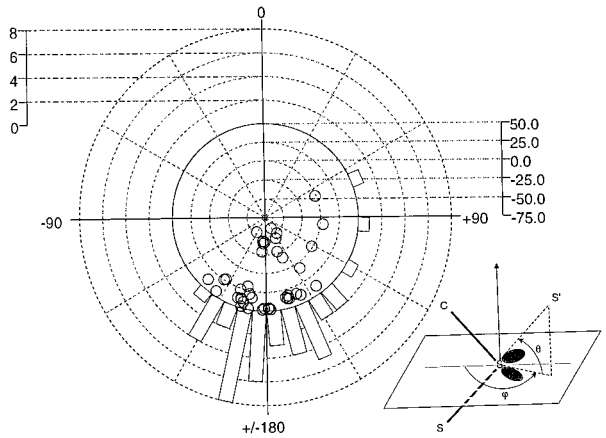

Figure 3. (a) Histogram of the S−S bonds length from CSD. Plots were generated using VISTA.[80] (b) Plot of the S−S bonds length versus the torsion angle C−S−S−C. (c) Polar histogram of θ versus φ from the CSD. Open symbols represent θ angles.

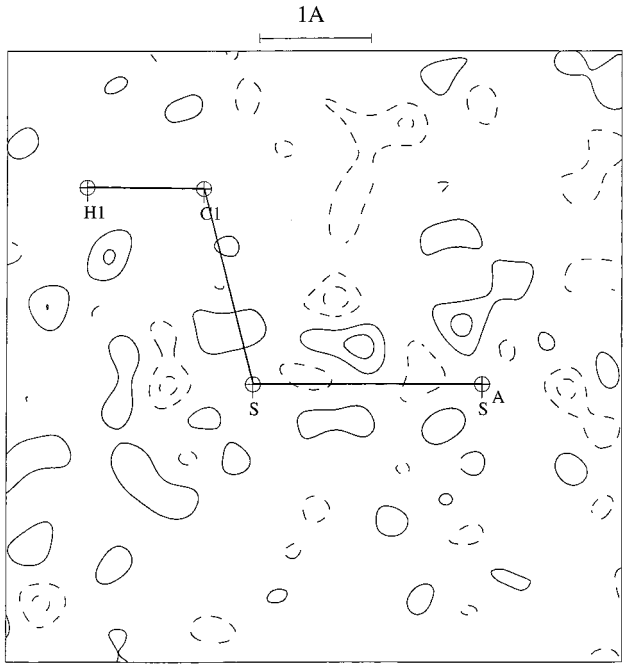

Figure 4. Residual electron density in the C1−S−S^{A} plane. Contours, 0.05 e Å^{-3}, negative dashed, no zero contour. The residual density map is calculated by Fourier synthesis according to $\Delta\rho_{res}(\mathbf{r}) = (1/V)\sum_{\mathbf{H}}$-$[|F_{obs}(\mathbf{H})| - |F_{mul}(\mathbf{H})|] \exp[i(\varphi_{mul} - 2\pi\mathbf{H}\cdot\mathbf{r})]$.

Table 5 gives κ, P_v, and the net atomic charges of atoms in L-cystine calculated from the Kappa refinement,[60] which is a model which does not include the nonspherical multipole functions. No chemical constraints were imposed on any atom, but electroneutrality of the cell was ensured. Opposite charges of −0.38 and +0.55 ē appear respectively on the COO and NH_3 groups, formally COO^- and NH_3^+. By comparison, those derived after multipolar refinement are −0.56 and +0.55 ē. The charge of +0.21(6) ē for the S atom is close to those obtained by ab initio calculations on a ClSSCl (0.156 ē) cluster using a 6-31G* basis set (Knop et al.[61]). The net charges can also be compared to the experimental charges of sulfur atoms in heptasulfur imide[11] (+0.22 ē) and to EHMO calculations on tetraethylthiuram disulfide[10](+0.19 ē). As expected from the positive charge of the sulfur atom, its κ parameter is greater than 1, close to 1.02, corresponding to a slight contraction of the electronic cloud. Like all negative oxygen atoms, the κ value of 0.98 for the oxygen atoms shows an expansion of the valence shell.

The calculation of the dipole moment in the asymmetric unit, with charges and atomic dipoles obtained at the end of the multipolar model and also with the net charges derived from Kappa refinement (Coppens and Hansen[62] and Espinosa et al.[63]), gives 10.4 (5) and 8.3 (5) D, respectively. The direction of the dipole moment is close to the COO^-/NH_3^+ direction for both refinements, the angles formed by this direction and the dipole vector being 7 and 3° respectively. The contribution of the polar groups COO^- and NH_3^+ is dominant in this compound: indeed, dipole moments calculated only with the contribution of COO^- and NH_3^+ groups are 9.8 (5) and 8.1 (5) D.

To characterize the chemical bonds in the title compound, we also have described the topology of the experimental static density.[64,65] The program NEWPROP developed by Souhassou and Blessing[66,67] was used to calculate the topology of the experimental electron density. The topological parameters of the electron density for the (3, −1) critical points (CPs) in L-cystine are given in Table 6 compared to those calculated with

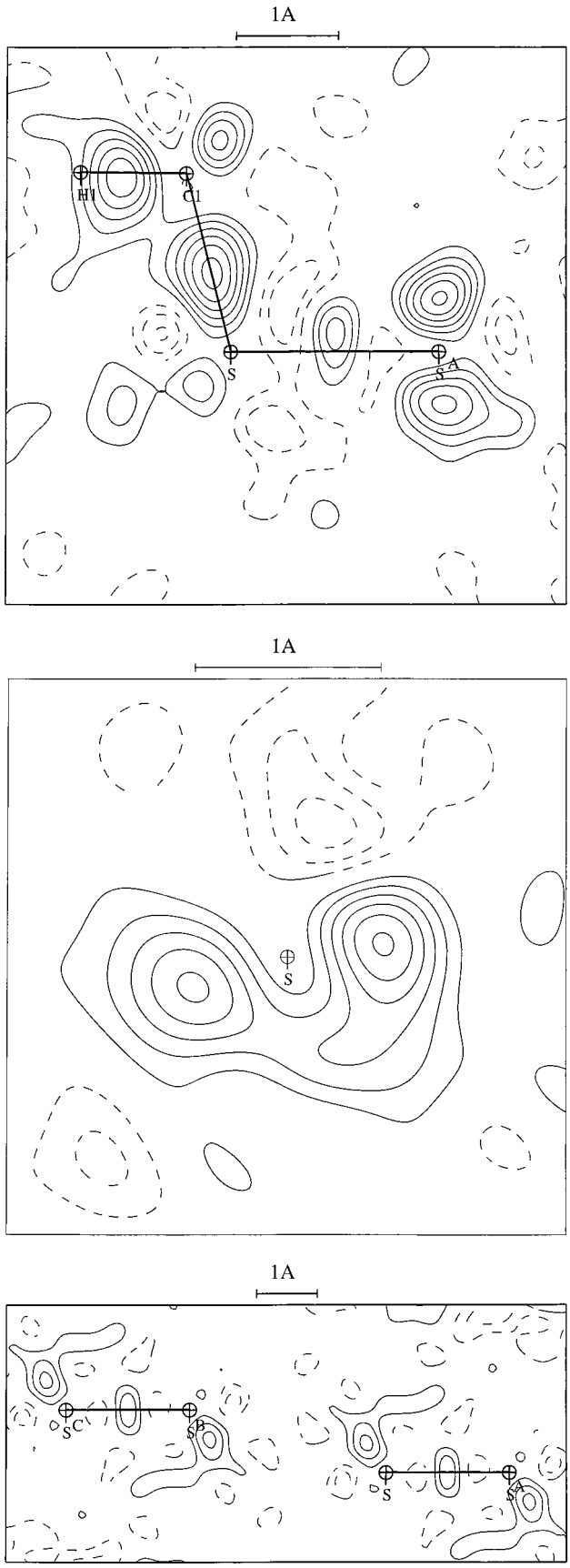

Figure 5. (a) Experimental deformation electron density $\Delta\rho_{exp}(\mathbf{r})$ in the C1−S−S^{A} plane. (b) $\Delta\rho_{exp}(\mathbf{r})$ in the bisecting plane of the C1−S−S^{A} angle. (c) $\Delta\rho_{exp}(\mathbf{r})$ in the plane containing the S−S bonds and the *c*-axis. Contours as in Figure 3. $\Delta\rho_{exp}(r)$ calculated by Fourier synthesis according to $\Delta\rho_{exp}(\mathbf{r}) = (1/V)\sum_{\mathbf{H}}[|F_{obs}(\mathbf{H})| \exp(i\varphi_{mul}) - |F_{sph}$-$(\mathbf{H})| \exp(i\varphi_{sph})] \exp(-2\pi i\mathbf{H}\cdot\mathbf{r})$.

TABLE 5: κ, P_v, and Net Charges in L-Cystine and Their esd's from the κ Refinement (First Line) and from the Multipole Refinement (Second Line)

atom	κ	P_v	net charge
S	1.017(6)	5.79(6)	+0.21(6)
	1.005(5)	5.91(6)	+0.09(6)
O1	0.983(5)	6.38(6)	−0.38(6)
	0.984(5)	6.25(6)	−0.25(6)
O2	0.979(4)	6.32(5)	−0.32(5)
	0.969(5)	6.34(6)	−0.34(6)
C1	0.99(1)	4.39(9)	−0.39(9)
	0.96(1)	4.54(9)	−0.54(9)
C2	0.99(1)	4.37(9)	−0.37(9)
	0.98(1)	4.20(9)	−0.20(9)
C3	1.05(1)	3.68(9)	+0.32(9)
	0.99(1)	3.98(9)	+0.02(9)
N	1.018(7)	5.21(7)	−0.21(7)
	0.979(7)	5.40(8)	−0.40(8)
H1	1.18(2)	0.91(3)	+0.09(3)
	1.10(2)	0.82(4)	+0.18(4)
H2	1.21(2)	0.87(3)	+0.13(3)
	1.14(2)	0.71(4)	+0.29(4)
H3	1.18(2)	0.84(3)	+0.16(3)
	1.12(2)	0.82(4)	+0.18(4)
H4	1.24(3)	0.78(3)	+0.22(3)
	1.25(2)	0.71(3)	+0.29(3)
H5	1.28(3)	0.75(3)	+0.25(3)
	1.21(2)	0.65(4)	+0.35(4)
H6	1.29(3)	0.72(3)	+0.28(3)
	1.24(3)	0.69(4)	+0.31(4)

the promolecule (i.e. superposition of free spherical neutral atoms). Parts a, b, and c of Figure 6 display, respectively, the negative Laplacian in the C1−S−S^A plane, in the plane bisecting the C1−S−S^A angle, and in the plane containing two S−S bonds and the *c*-axis. Figure 7 gives the gradient vector field of the electron density $\nabla\rho(\mathbf{r})$. This figure, which gives the atomic basins and the trajectories associated with the (3, −1) CPs, shows very well the one-dimensional S−S···S interactions which run along [0 1 0]. The most negative $\nabla^2\rho(\mathbf{r}_c)$ and the highest $\rho(\mathbf{r}_c)$ values are found for the C3···O1 and C3···O2 CPs. The slight discrepancy between both C···O characteristics (Table 6) is a consequence of the difference observed between the C ···O bond lengths (0.022 Å) due to the presence of a double hydrogen bond for O2. Previous experimental high-resolution studies on small molecules[63,68−73] led to the mean values of $[\nabla^2\rho(\mathbf{r}_c), \rho(\mathbf{r}_c)]$ at the CP: [−28.26 ± 6.14 e Å^{-5}, 2.78 ± 0.12 e Å^{-3}] for C···O, [−13.75 ± 4.33 e Å^{-5}, 1.95 ± 0.30 e Å^{-3}] for C−N, and [−12.37 ± 0.84 e Å^{-5}, 1.68 ± 0.06 e Å^{-3}] for C−C. These results are in excellent agreement with those obtained for L-cystine.

Compared to the promolecule, the positions of the CP involving the S atoms do not change but their density increases and the Laplacian becomes slightly less than zero. The CP of the S−C1 bond is closer to the carbon atom due to their respective atomic volumes. The $\nabla^2\rho(\mathbf{r}_c)$, $\rho(\mathbf{r}_c)$, and ϵ of −5.68 e Å^{-5}, 1.21 e Å^{-3}, and 0.09, respectively, are characteristic of a covalent atomic interaction for which the density is concentrated in the S−C1 bond. The two negative (λ_1, λ_2) curvatures at the CP are of equal magnitudes and the ratio $|\lambda_3/\lambda_1|$ close to 1 indicates that the S−C1 bond has a cylindrical symmetry. Very close experimental values of the Laplacian and of the electron density at the CP were obtained in other compounds containing S−C bonds: [−2.39 e Å^{-5}, 1.34 e Å^{-3}] and [−3.10 e Å^{-5}, 1.31 e Å^{-3}] in the BTDMTTF−TCNQ complex,[48] [−6.82 e Å^{-5}, 1.33 e Å^{-3}] in 3,3,6,6-tetramethyl-*S*-tetrathiane,[14] [−2.60 e Å^{-5}, 1.36 e Å^{-3}] and [−2.00 e Å^{-5}, 1.39 e Å^{-3}] in diaryl(alkoxy)acyloxy)spiro-λ^4-sulfane[74] compared to +2.58 e Å^{-5} and 0.89 e Å^{-5} for noninteracting atoms. The two latter cases correspond to a methyl-substituted six-membered ring containing four sulfur atoms, one adopting a twist-boat conformation, and the other with an hypervalent bond.

The S−S bond in the title compound has a negative Laplacian at the critical point; i.e., the atoms are bound by a shared concentration of charge. As shown in Figure 6, the valence shell charge concentration (VSCC) of the S atom is strongly polarized toward the nearby S and C atoms (bonded charge concentration) and presents additional maxima in the VSCC corresponding to the lone-pair electrons (Lp) (nonbonded charge concentration) in accordance with the Lewis model.[75] These lone pair features at ∼ 0.7 Å from the nucleus are exactly located in the plane bisecting the C1−S−S^A angle. Their topological $\nabla^2\rho$ minima form a Lp$_1$−S−Lp$_2$ angle of 145° (Figure 6b). This distribution of the VSCC of the S atom is therefore close to a sp^3

TABLE 6: Topological Parameters of Bonds in L-Cystine Compared to the Promolecule Model[a]

bonds	d_1	d_2	λ_1	λ_2	λ_3	$\nabla^2\rho(\mathbf{r}_c)$	$\rho(\mathbf{r}_c)$	ϵ	$\lvert\lambda_3/\lambda_1\rvert$
S−S^A	1.025	1.025	5.39	−4.32	−3.63	−2.57	0.89	0.20	0.67
	1.025	1.025	7.98	−2.57	−2.57	2.84	0.77	0.00	0.32
S−C1	0.971	0.847	7.37	−6.23	−6.82	−5.68	1.21	0.09	0.93
	0.971	0.847	9.23	−3.31	−3.34	2.58	0.89	0.01	0.36
C3−O2	0.478	0.788	26.53	−23.18	−25.75	−22.40	2.65	0.11	0.97
	0.503	0.763	28.22	−11.87	−12.11	4.24	2.02	0.02	0.43
C3−O1	0.488	0.757	24.93	−25.08	−27.34	−27.50	2.86	0.09	1.10
	0.489	0.755	30.69	−12.59	−12.82	5.27	2.09	0.02	0.42
C2−C3	0.763	0.775	10.60	−11.11	−12.74	−13.25	1.76	0.146	1.20
	0.769	0.769	11.72	−4.86	−4.98	1.87	1.12	0.02	0.42
C2−N	0.628	0.853	13.45	−9.88	−10.82	−7.25	1.54	0.10	0.80
	0.675	0.805	17.40	−6.70	−6.72	3.98	1.35	0.00	0.39
C1−C2	0.763	0.761	9.93	−10.53	−10.98	−11.58	1.68	0.04	1.11
	0.761	0.762	11.82	−5.07	−5.08	1.67	1.15	0.00	0.43
S···S^B	1.717	1.717	0.90	−0.15	−0.23	0.53	0.08	0.50	0.26
	1.717	1.717	0.83	−0.12	−0.13	0.58	0.07	0.05	0.16
N−H4···O2^C	0.599	1.183	5.92	−0.99	−1.01	3.92	0.21	0.03	0.17
	0.694	1.083	6.98	−1.59	−1.71	3.68	0.32	0.08	0.24
N−H6···P2^D	0.693	1.236	3.94	−0.70	−0.77	2.47	0.16	0.09	0.20
	0.771	1.139	5.11	−1.10	−1.13	2.88	0.23	0.02	0.22
N−H5···O1^G	0.662	1.185	4.71	−0.93	−0.95	2.82	0.20	0.02	0.20
	0.735	1.109	5.96	−1.36	−1.38	3.21	0.27	0.01	0.23

[a] $\nabla^2\rho(\mathbf{r}_c)$ and $\rho(\mathbf{r}_c)$ Denote the Laplacian (e Å^{-5}) and the Electron Density (e Å^{-3}) at the (3, −1) CP; ϵ is the bond ellipticity. d_1 and d_2 are the distances (Å) from the CP to each atom, and λ_1, λ_2, and λ_3 are the eigenvalues of the Hessian matrix from the multipolar model (top).

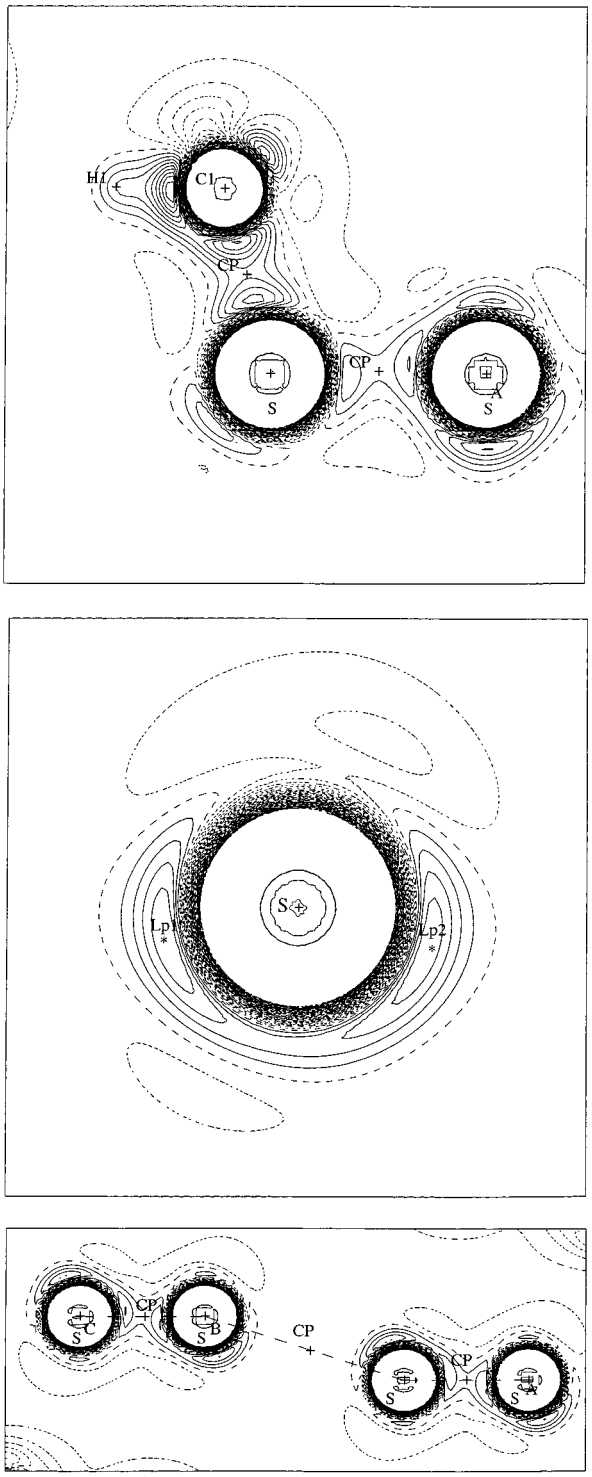

Figure 6. (a) Negative Laplacian of the electron density in the same plane as in Figure 5a. (b) Negative Laplacian in the same plane as in Figure 5b. **(**c) Negative Laplacian in the same plane as in Figure 5c. Contours at ±2 e Å^{-5}.

hybridization (a sp^2 hybridization would show one single extremum in the C1−S−S^A plane). Because the two sulfur atoms are related by 2-fold axes parallel to [1 0 0] or [1 1 0] directions which run through the midpoint of the S−S bond, the (3, −1) CP of the S−S bond is at the special position equidistant from each nucleus. The density at the critical point (0.89 e Å^{-3}) and its ϵ value (0.20) are also characteristic of a shared shell interaction. A comparison of S−S covalent bond topological parameters is given in Table 7, most of these being theoretical calculations. The calculated values of the Laplacian

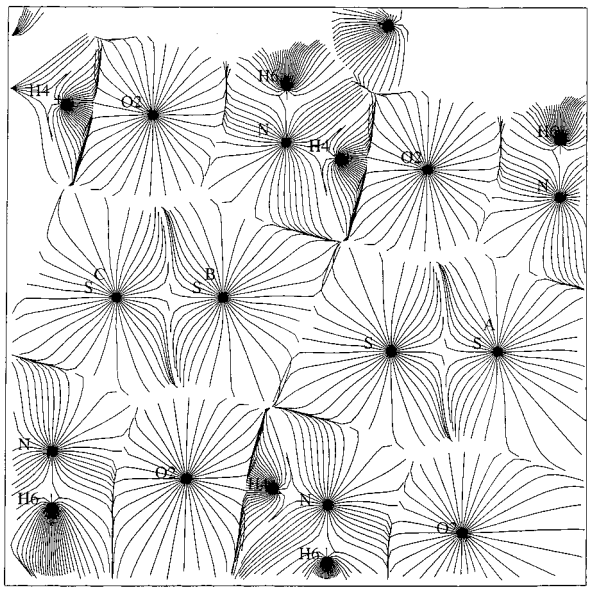

Figure 7. $\vec{\nabla}\rho(r)$ gradient vector field of the electron density in the plane containing the S−S bonds. S···S^B bond is along the [010] direction.

TABLE 7: Bond Distances (Å), Laplacian (e Å^{-5}), and Electron Density (e Å^{-3}) for S−S Bonds at the (3, −1) CP

molecule	S−S	$\nabla^2\rho(\mathbf{r}_c)$	$\rho(\mathbf{r}_c)$	method	ref
L-cystine	2.0472(4)	−2.57	0.89	experimental	this work
S_4^{2+}	2.06	−1.71	0.86	theoretical	5
	1.99	−7.86	1.23	theoretical	5
H_2S_2	2.06	−1.59	0.81	theoretical	5
		−4.70	1.01	theoretical	5
	2.063		1.00	theoretical	14
	2.0633		1.00	theoretical	62
S_8	2.07	−1.40	0.84	theoretical	5
S_8^{2+}	2.06	−1.01	0.80	theoretical	5
S_8^{4+}	2.08	−0.58	0.80	theoretical	5
$[(CH_3)_2CS_2]_2$	2.023(1)	−0.59	1.13	experimental	14
		−5.39	1.09	theoretical	14
S_2	1.878		1.39	theoretical	14
F_2S_2	1.9534		1.28	theoretical	62
Cl_2S_2	2.0040		1.14	theoretical	62

at CP show pronounced variation due to the different S−S bond lengths ($-7.86 < \nabla^2\rho(\mathbf{r}_c) < -0.58$ e Å^{-5}, for 1.99 < S−S < 2.08 Å). Taking into account the bond lengths, our experimental result of the $\nabla^2\rho(\mathbf{r}_c)$ and $\rho(\mathbf{r}_c)$ are in excellent agreement with these theoretical calculations. In addition, the values of $\rho(\mathbf{r}_c)$ are in line with Knop et al.[61] work concerning the relationship between S−S bond length and the electron density at the CP.

IV.3. Intermolecular Interactions. Topological parameters, characteristic of intermolecular interactions, are also listed in Table 6. The O2 atom is an acceptor for two hydrogen bridges (O_2···H4 = 1.777 (1) Å and O_2···H6 = 1.910 (1) Å), and O1 accepts one hydrogen bond (O_1···H5 = 1.844 (1) Å). The kinetic energy density *G(r)* at the CP can be estimated according to Abramov's function[76] for closed-shell interactions. Values of 94.35, 59.58, and 72.57 kJ/mol per atomic unit volume are obtained for N−H4···O2, N−H6···O2, and N−H5···O1, respectively. These energy densities are in excellent agreement with those obtained recently from our statistical analysis of the topological properties of the experimental hydrogen bond strength electron density.[77−79]

Figure 6c shows the S···S^B intermolecular interaction. There is a (3, −1) CP located between the two S atoms which exhibits characteristics similar to the dimer of L-cystine promolecules (Table 6). The charge density (0.02−0.03 e Å^{-3}) and the

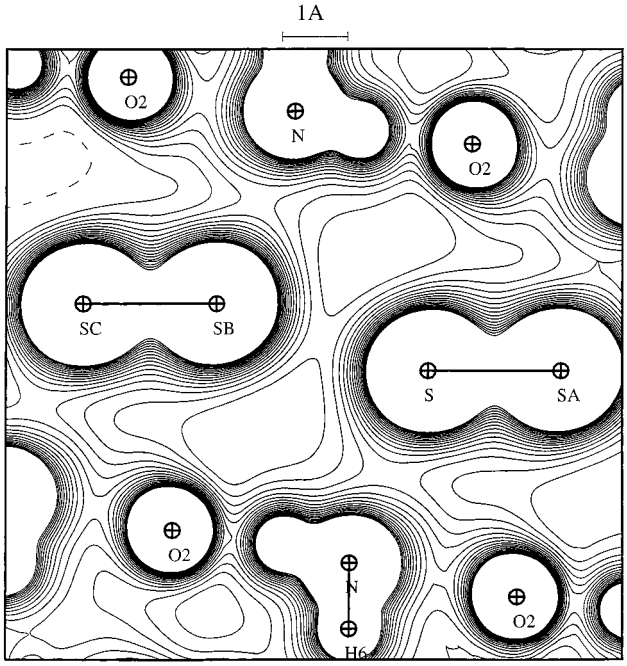

Figure 8. Electrostatic potential in the same plane as in Figure 6b. Contours intervals are at 0.05 e Å^{-1}.

Laplacian (0.36−0.53 e Å^{-5}) are also the same than those found for O···O van der Waals contacts in experimental charge density pentafluorosulfanyl isocyanate[80] (F_5SNCO). The valence shell charge concentration corresponding to the lone pairs is not polarized toward the intermolecular direction (Figure 6c). The same features are also revealed by the deformation density map (Figure 5c). The kinetic energy density at the S···S CP calculated as above gives 14.26 kJ/mol per atomic unit volume. This result is close to that obtained for the reference van der Waals compound (Ar···FH; 16.74, kJ/mol per atomic unit volume),[65] and smaller than those obtained for the hydrogen bonds.[77−79] Another way to visualize interactions is to determine the intermolecular electrostatic potential. Figure 8 gives the electrostatic potential in the same plane as in Figure 6c calculated with ELECTROS program.[81] It reveals the region of maximum interaction of the S atoms: the positive potential region around the S atoms divides into two parts on each side of the S···S contact line. This leads to a flat valley of slightly positive potential (+ 0.055 e Å^{-1}) corresponding to an electrostatic energy of 76.40 kJ/mol (18.28 kcal/mol) for a positive unit point charge.

V. Conclusion

This work establishes the feasibility of experimental diffraction studies with a CCD-equipped diffractometer on crystals having large unit cell parameters: we have shown that precise electron density and related electronic properties of L-cystine can be now obtained with excellent accuracy in a much shorter time by using high-resolution low-temperature X-ray diffraction data from a CCD area detector. However, this demands very careful data collection and data reduction. In terms of the charge density topology, it is clear now that S−S bonds are weak single covalent bonds. The almost tetrahedral distribution of the VSCC of the sulfur atom is consistent with sp^3 hybridization. The structure of L-cystine is stabilized by hydrogen bonds linking molecules via COO^- and NH_3^+ as shown by the dominant contribution of these groups in the calculation of the dipolar moment. The topological characteristics of S···S classify the interaction as van der Waals type. Other experimental studies of sulfur-containing molecules are in progress and will be published soon.

Acknowledgment. EPSRC for a Research Fellowship for S.D., the Royal Society (UK), and CNRS (France) for the financial support for the Alliance Project are gratefully acknowledged. We thank Dr. R. H. Blessing for providing the new SORTAV version and for the fruitful recommendations to use it. We also are very grateful to Drs. C. Wilson, A.E. Goeta, D.S. Yufit, N.E. Ghermani, and M. Souhassou for helpful discussions.

Supporting Information Available: Tables listing fractional coordinates, anisotropic thermal displacement parameters of the final converged spherical, HO, and multipolar model, agreement indices for S radial functions, local atom-centered cartesian axes used in the MOLLY program, and multipolar parameters of the final converged multipolar model; figures showing experimental static deformation densities (10 pages). This material is available free of charge via the Internet at http://pubs.acs.org.

References and Notes

(1) Huxtable, R. J. *Biochemistry of Sulfur*; Plenum Press: New York, 1986.
(2) Coppens, P.; Yang, Y. W.; Blessing, R. H.; Cooper, W. F.; Larsen, F. K. *J. Am. Chem. Soc*. **1977**, *99*, 760.
(3) Kirfel, A.; Will, G. *Acta Crystallogr*. **1980**, *B36*, 512.
(4) Elerman, Y.; Bats, J. W.; Fuess, H. *Acta Crystallogr*. **1983**, *C39*, 515.
(5) Tang, T. H.; Bader, R. F. W.; MacDougall, P. J. *Inorg. Chem*. **1985**, *24*, 2047.
(6) Wang, Y.; Chen, M. J.; Wu, C. H. *Acta Crystallogr*. **1988**, *B44*, 179.
(7) Wang, Y.; Liao, J. H. *Acta Crystallogr*. **1989**, *B45*, 65.
(8) Wang, Y.; Wu, S. Y.; Cheng, A. C. *Acta Crystallogr*. **1990**, *B46*, 850.
(9) Wang, Y.; Yeh, S. K.; Wu, S. Y.; Pai, C. T.; Lee, C. R.; Lin, K. J. *Acta Crystallogr*. **1991**, *B47*, 298.
(10) Yeh, S. K.; Wang, Y. *Acta Crystallogr*. **1992**, *B48*, 319.
(11) Wang, C. C.; Hong, Y. Y.; Ueng, C. H.; Wang, Y. *J. Chem. Soc., Dalton Trans*. **1992**, 331.
(12) Lin, K. J.; Wang, L. *J. Phys. Chem*. **1993**, *97*, 3176.
(13) Brown, A. S.; Smith Jr., V. H. *J. Chem. Phys*. **1993**, *99*, 1837.
(14) McCormack, K. L.; Mallinson, P. R.; Webster, B. C.; Yufit, D. S. *J. Chem. Soc. Faraday Trans*. **1996**, *92* (10), 1709.
(15) Gleiter, R.; Hoffman, R. *Tetrahedron* **1968**, *24*, 5899.
(16) Ratner, M. A.; Sabin, J. R. *J. Am. Chem. Soc*. **1977**, *99*, 3954.
(17) Cohen-Addad, C.; Lehman, M. S.; Becker, P.; Parkanyi, L.; Kalman, A. *J. Chem. Soc., Perkin Trans. 2* **1984**, 191.
(18) Pichon-Pesme, V.; Lecomte, C.; Lachekar, H. *J. Phys. Chem*. **1995**, *99*, 6246.
(19) Jelsch, C.; Pichon-Pesme, V.; Lecomte, C.; Aubry. A. *Acta Crystallogr*. **1998**, *D54*, 1306.
(20) Coppens, P.; Carducci, M.; Bolotovsky, R.; Zeleski, J. XI Sagamore Conference (Prince Albert, Canada),1997; RA52, 65.
(21) Pinkerton, A. A. XI Sagamore Conference (Prince Albert, Canada), 1997; RM50, 63.
(22) Koritsanszky, T.; Flaig, R.; Zobel, D.; Krane, H.-G.; Morgenroth, W.; Luger, P. *Science* **1998**, *279*, 356.
(23) Graafsma, H.; Souhassou, M.; Puig-Molina, A.; Harkema, S.; Kvick, A.; Lecomte, C. *Acta Crystallogr*. **1998**, *B54*, 193.
(24) Kuntzinger, S., Dahaoui, S.; Ghermani, N. E., Lecomte, C.; Howard, J. A. K.; *Acta Crystallogr*. **1999**, *B55*, 000.
(25) Dahaoui, S.; Jelsch, C.; Howard, J. A. K.; Lecomte, C. *Acta Crystallogr*. **1999**, *B55*, 226.
(26) Martin A.; Pinkerton A. A. *Acta Crystallogr*. **1998**, *B54*, 471.
(27) Macchi P.; Proserpio, D. M.; Sironi, A.; Soave, R.; Destro, R. *J. Appl. Crystallogr*. **1998**, *31*, 583.
(28) Siemens. *ASTRO* and *SAINT*: *Data Collection and Processing Software for the SMART System*. Siemens Analytical X-ray Instruments Inc.: Madison, WI, 1995.
(29) Kabsch, W. *J. Appl. Crystallogr*. **1993**, *26*, 795.
(30) Sheldrick, G. M. *SADABS*: *Siemens Area Detector Absorption Correction Program*; University of Göttingen, Germany, 1996.
(31) De Titta, G. *J. Appl. Crystallogr*. **1985**, *18*, 75.
(32) Blessing, R. H. *Crystallogr. Rev*. **1987**, *1*, 3. New version 1998 to be published.

(33) Abrahams, S. C.; Keve, E. T. *Acta Crystallogr*. **1971**, *A27*, 157.
(34) Rees, B. *Isr. J. Chem*. **1977**, *16*, 154 and 180.
(35) French, S.; Wilson, K. *Acta Crystallogr*. **1978**, *A34*, 517.
(36) Oughton, B. M.; Harrison, P. M. *Acta Crystallogr*. **1959**, *12*, 396.
(37) Sheldrick, G. M. *Acta Crystallogr*. **1990**, *A46*, 467.
(38) Sheldrick, G. M. *SHELXL93*: *Program for the refinement of Crystal Structures*; University of Göttingen, Germany, 1993.
(39) Flack, H. D. *Acta Crystallogr*. **1983**, *A39*, 876.
(40) Hirschfeld, F. L. *Acta Crystallogr*. **1976**, *A32*, 239.
(41) Becker, P.; Coppens, P. *Acta Crystallogr*. **1974**, *A30*, 129.
(42) Allen, F. H. *Acta Crystallogr*. **1986**, *B42*, 515.
(43) Hansen, N. K.; Coppens, P. *Acta Crystallogr*. **1978**. *A34*, 909.
(44) El Haouzi, A.; Hansen, N. K.; Le Hénaff, C.; Protas, J. *Acta Crystallogr*. **1996**, *A52*, 291.
(45) Clementi, E.; Raimondi, D. L. *J. Chem. Phys*. **1963**, *38*, 2686.
(46) Stewart, R. F. *Isr. J. Chem*. **1977**, *16*, 124.
(47) Moss, G. R.; Souhassou, M.; Blessing, R. H.; Espinosa, E.; Lecomte, C. *Acta Crystallogr*. **1995**, *B51*, 650.
(48) Espinosa, E.; Molins, E.; Lecomte, C. *Phys. Rev. B* **1997**, *56* (4), 1820.
(49) Hehre, W. J.; Ditchfield, R.; Stewart, R. F.; Pople, J. A. *J. Chem. Phys*. **1970**, *52*, 2769.
(50) Koritsanszky, T.; Howard, S. T.; Mallinson, P. R.; Su, Z.; Richter, T.; Hansen, N. K. *XD*: *Computer program package for multipole refinement and analysis of charge densities from diffraction data*. Free University of Berlin. Germany, 1995.
(51) Jonhson, C. K. *ORTEPII*. Report ORNL-5138; Oak Ridge National Laboratory, TN, 1976.
(52) Allen, F. H.; Davies, J. E.; Galloy, J. J.; Johnson, O.; Kennard, O.; Macrae, C. F.; Mitchell, E. M.; Mitchell, G. F.; Smith, J. M.; Watson, D. G. *J. Chem. Inf. Comput. Sci*. **1991**, *31*, 187.
(53) Allen, F. H.; Bird, C. M.; Rowland, R. S.; Raithby, P. R. *Acta Crystallogr*. **1997**, *B53*, 696.
(54) Rosenfield, R. S.; Parthasarathy, R.; Dunitz, J. D. *J. Am. Chem. Soc*. **1977**, *99*, 4860.
(55) Hirschfeld, F. L. *Acta Crystallogr*. **1971**, *B27*, 769.
(56) Stevens, E. D.; Rys, J.; Coppens, P. *J. Am. Chem. Soc*. **1978**, *100*, 2324.
(57) Swaminathan, S.; Craven, B. M.; Spackman, M. A.; Stewart, R. F. *Acta Crystallogr*. **1984**, *B40*, 398.
(58) Lecomte, C.; Ghermani, N. E.; Pichon-Pesme, V.; Souhassou. M. *J. Mol. Struct*. **1992**, *255*, 241.
(59) Souhassou, M.; Lecomte, C.; Blessing, R. H.; Aubry, A.; Rohmer, M. M.; Wiest, R.; Bénard, M. *Acta Crystallogr*. **1991**, *B47*, 253.
(60) Coppens, P.; Guru, T. N.; Leung, P.; Stevens, E. D.; Becker, P.; Yang, Y. W. *Acta Crystallogr*. **1979**, *A35*, 63.
(61) Knop, O.; Boyd, R. J.; Choi, S. C. *J. Am. Chem. Soc*. **1988**, *110*, 7299.
(62) Coppens, P.; Hansen, N. K. *Isr. J. Chem*. **1977**, *16*, 163.
(63) Espinosa, E.; Lecomte, C.; Mollins, E.; Veintemillas, S.; Cousson, A.; Paulus, W. *Acta Crystallogr*. **1996**, *B52*, 519.
(64) Bader, R. F. W.; Essen, H. *J. Chem. Phys*. **1984**, *80*, 1943.
(65) Bader, R. F. W. *Atoms in molecules: A Quantum Theory*; Oxford Science Publications: Oxford, UK, 1990.
(66) Souhassou, M.; Blessing, R. H. *J. Appl. Crystallogr*. **1999**, *32*, 210.
(67) Souhassou, M. *NEWPROP*: *Computer program to calculate the experimental multipolar electron density from high-resolution X-ray diffraction*; Internal Report CNRS UPRESA 7036, Université Henri Poincaré, Nancy 1, France, 1997.
(68) Stewart, R. F. *The Application of Charge Density Research to Chemistry and Drug Design*; Jeffrey, G. A., Piniella, J. F., Eds.; Nato ASI Series B 250; Plenum Press: New York and London, 1990; p 63.
(69) (a) Lachekar, H. Ph.D. Thesis, Université Henri Poincaré, Nancy 1, France, 1997.
(70) Flaig, R.; Koritsanszky, T.; Zobel, D.; Luger, P. *J. Am. Chem. Soc*. **1998**, *120*, 2227.
(71) Gatti, C.; Bianchi, R.; Destro, R.; Merati, F. *J. Mol. Struct. (THEOCHEM)* **1992**, *255*, 409.
(72) Flensburg, C.; Larsen, S.; Stewart, R. F. *J. Phys. Chem*. **1995**, *99*, 10130.
(73) Howard, S. T.; Hursthouse, M. B.; Lehmann, C. W.; Poyner, E. A. *Acta Crystallogr*. **1995**, *B51*, 328.
(74) Szabó, D.; Kapovits, I.; Argay, Gy.; Czugler, M.; Kálmán, A.; Koritsanszky, T. *J. Chem. Soc., Perkin. Trans*. 2 **1997**, 1045.
(75) (a) Lewis, G. N. *J. Am. Chem. Soc*. **1916**, *38*, 762. (b) Lewis, G. N. *J. Phys. Chem*. **1933**, *1*, 17.
(76) Abramov, Yu. A. *Acta Crystallogr*. **1997**, *A53*, 264.
(77) Espinosa, E.; Molins, E.; Lecomte, C. *Chem. Phys. Lett*. **1998**, *285*, 170.
(78) Espinosa, E.; Souhassou, M.; Lachekar, H.; Lecomte, C. *Acta Crystallogr*. **1999**, 000.
(79) Espinosa, E.; Lecomte, C., Molins, E..*Chem. Phys. Lett*. **1999**, *300*, 745.
(80) Koritsanszky, T. *Intermolecular Interactions*, Gans, W., Boeyens, J. C. A., Eds.; Plenum Press: New York and London, 1997; pp 57−70.
(81) Ghermani, N. E.; Bouhmaida, N.; Lecomte, C. *ELECTROS*: *Computer program to calculate electrostatic properties from high-resolution X-ray diffraction*. Internal report URA CNRS 809, Université Henri Poincaré, Nancy 1, France, 1992.
(82) Allen, F. H.; Kennard, O. *Chem. Des. Automation News* **1993**, *8* (1), 1 and 31.